Short Article

Cell Metabolism

Mic10 Oligomerizes to Bend Mitochondrial Inner Membranes at Cristae Junctions

Graphical Abstract

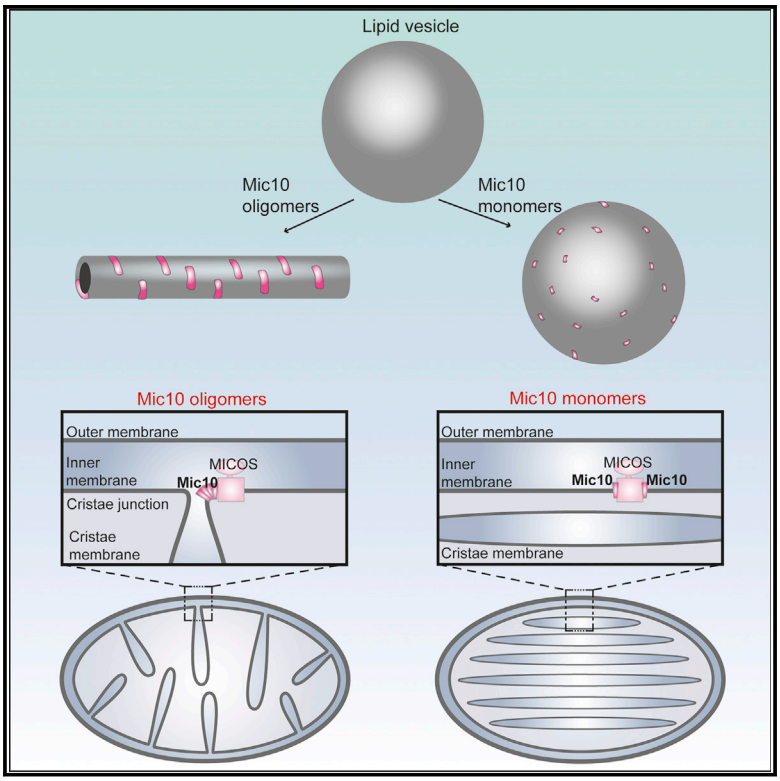

Authors

Mariam Barbot, Daniel C. Jans, ..., Stefan Jakobs, Michael Meinecke

Correspondence

michael.meinecke@med.uni-goettingen.de

In Brief

The mitochondrial inner membrane displays a complex architecture with tubular cristae invaginations and narrow openings, termed cristae junctions. Barbot et al. and Bohnert et al. show that the inner membrane protein Mic10 forms large oligomers and induces membrane curvature to orchestrate the formation of cristae junctions in mitochondria.

Highlights

- MICOS core subunit Mic10 induces high degrees of curvature in model membranes
- Mic10 forms homo-oligomers via two glycine-rich motifs
- Oligomerization of Mic10 is a prerequisite for membrane bending
- Membrane bending by Mic10 is necessary for cristae junction formation in mitochondria

Barbot et al., 2015, Cell Metabolism *21*, 756–763
May 5, 2015
http://dx.doi.org/10.1016/j.cmet.2015.04.006

CellPress

CellPress

Cell Metabolism
Short Article

Mic10 Oligomerizes to Bend Mitochondrial Inner Membranes at Cristae Junctions

Mariam Barbot,[1] Daniel C. Jans,[3,5] Christian Schulz,[1] Niels Denkert,[1] Benjamin Kroppen,[1] Michael Hoppert,[4] Stefan Jakobs,[3,5] and Michael Meinecke[1,2,*]
[1]Department of Cellular Biochemistry, University Medical Center Göttingen, 37073 Göttingen, Germany
[2]European Neuroscience Institute Göttingen, 37077 Göttingen, Germany
[3]Department of NanoBiophotonics, Max Planck Institute for Biophysical Chemistry, 37077 Göttingen, Germany
[4]Institute of Microbiology and Genetics, Georg-August-University, 37077 Göttingen, Germany
[5]Department of Neurology, University Medical Center, 37075 Göttingen, Germany
*Correspondence: michael.meinecke@med.uni-goettingen.de
http://dx.doi.org/10.1016/j.cmet.2015.04.006

SUMMARY

The mitochondrial inner membrane is highly folded and displays a complex molecular architecture. Cristae junctions are highly curved tubular openings that separate cristae membrane invaginations from the surrounding boundary membrane. Despite their central role in many vital cellular processes like apoptosis, the details of cristae junction formation remain elusive. Here we identify Mic10, a core subunit of the recently discovered MICOS complex, as an inner mitochondrial membrane protein with the ability to change membrane morphology in vitro and in vivo. We show that Mic10 spans the inner membrane in a hairpin topology and that its ability to sculpt membranes depends on oligomerization through a glycine-rich motif. Oligomerization mutants fail to induce curvature in model membranes, and when expressed in yeast, mitochondria display an altered inner membrane architecture characterized by drastically decreased numbers of cristae junctions. Thus, we demonstrate that membrane sculpting by Mic10 is essential for cristae junction formation.

INTRODUCTION

Organellar membranes display a multitude of shapes. However, the factors and mechanisms by which these shapes are created are largely unknown. Mitochondria possess two membranes of different function and architecture. The highly folded inner membrane (IM) can be divided into functional regions, which display different degrees of membrane curvature (Figure 1A). Cristae membranes, the invaginations of the inner boundary membrane toward the matrix, can adopt a variety of different shapes, from lamellar sheet-like to tubular-like structures (Scheffler, 2007). Interestingly, although cristae membranes are diverse in size and shape (Zick et al., 2009), cristae junctions (CJs), which separate cristae from the flat boundary membrane, appear rather uniform. They are narrow, short tubular openings that typically display inner diameters between 15 and 40 nm (Mannella, 2006). CJs are believed to have profound implications for the regulation of mitochondrial processes like apoptosis and energy conversion by restricting the free diffusion of proteins, ions, and metabolites along the IM and thereby forming or maintaining functional sub-domains within the IM and the intermembrane space (Mannella, 2006; Pellegrini and Scorrano, 2007; Rabl et al., 2009; Scorrano et al., 2002; Strauss et al., 2008; Vogel et al., 2006). The formation of CJs, particularly how membrane bending to the degree observed at CJs occurs, is poorly understood. Recent studies have identified the evolutionary conserved, multi-subunit, MICOS complex (*mi*tochondrial *c*ontact site and cristae *o*rganizing *s*ystem) (Harner et al., 2011; Hoppins et al., 2011; Pfanner et al., 2014; von der Malsburg et al., 2011), which is enriched at CJs (Harner et al., 2011; Jans et al., 2013; Rabl et al., 2009). Decreased expression levels of MICOS subunits cause drastic changes in inner mitochondrial membrane morphology and lead to a highly decreased number of CJs. Consequently, cristae membranes are detached from the rest of the IM and appear as stacks within the mitochondrial matrix (Alkhaja et al., 2012; Harner et al., 2011; Hoppins et al., 2011; John et al., 2005; von der Malsburg et al., 2011). Whether MICOS proteins are actively shaping CJs, and the molecular mechanism by which they would do so, is not known.

RESULTS

Mic10 Induces High Degrees of Membrane Curvature in Model Membranes

Depletion of Mic10, a core subunit of the MICOS complex, leads to a massive loss of CJs and abnormal cristae structures (Alkhaja et al., 2012; Harner et al., 2011; Hoppins et al., 2011; von der Malsburg et al., 2011). To investigate this protein and its role in CJ formation, we expressed and purified *S. cerevisiae* Mic10 from *E. coli* to homogeneity (Figure 1B). Mic10 was solubilized in n-Dodecyl β-D-maltoside (DDM) and integrated into large unilamellar vesicles (LUVs) using a detergent-mediated reconstitution protocol (Meinecke et al., 2006). Reconstitution success was monitored by flotation assays (Figures 1C and 1D), and membrane integration of the protein was confirmed by subsequent carbonate extraction (Figure 1E). Interestingly, when compared to flotation patterns of empty LUVs, Mic10-containing

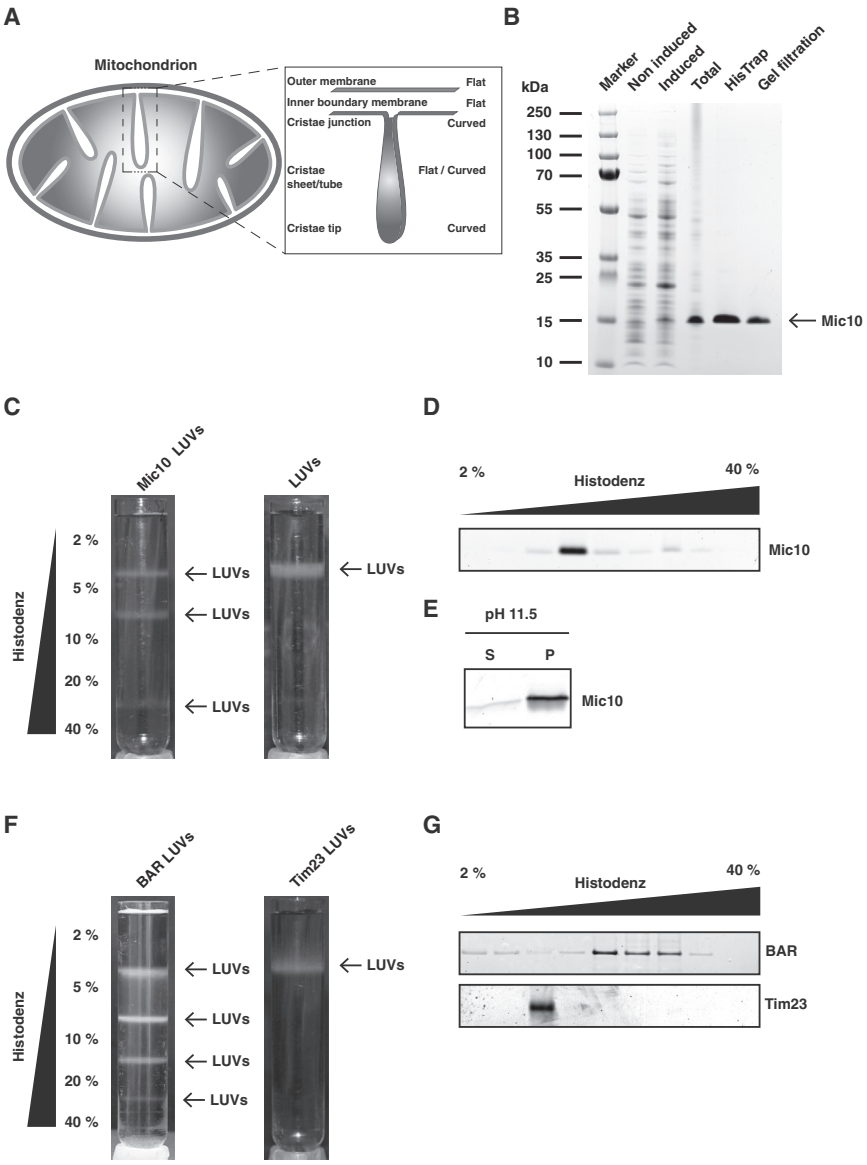

Figure 1. Recombinant Mic10 Can Be Reconstituted into LUVs

(A) Schematic view of a mitochondrion, with focus on the ultra-structure of the inner membrane.

(B) Expression and purification of recombinant Mic10 analyzed by SDS-PAGE with Coomassie brilliant blue staining.

(C) Flotation assay of empty LUVs (right) and vesicles with incorporated Mic10 (left) separated on a Histodenz gradient.

(D) Fractionation of flotated Mic10 (see C, left gradient) analyzed by SDS-PAGE with Coomassie brilliant blue staining.

(E) Sodium-carbonate extraction assay of Mic10-containing LUVs analyzed by SDS-PAGE with Coomassie brilliant blue staining.

(F) Flotation assay of LUVs in the presence of endophilin BAR domain (left) and vesicles with incorporated Tim23 (right).

(G) Fractionation of flotated BAR and Tim23 analyzed by SDS-PAGE with Coomassie brilliant blue staining.

vesicles were found at various densities of the gradient (Figures 1C and 1D), suggesting that Mic10 changes the overall structure of LUVs. Similar flotation patterns could be observed when LUVs were incubated with the BAR domain of endophilin (Figures 1F and 1G), a protein known to induce high degrees of membrane curvature (Farsad et al., 2001; Gallop et al., 2006; Meinecke et al., 2013) (Figure S1C). LUVs containing the mitochondrial IM translocase Tim23, a protein predominantly localized in the boundary membrane but not involved in membrane remodeling processes, showed flotation patterns very similar to empty vesicles (Figures 1F and 1G).

To directly analyze Mic10-induced changes in membrane morphology, we used electron microscopy on LUVs (Figure 2A). Mic10-containing vesicles showed broad structural changes in LUV membrane morphology. We repeatedly observed tubular membrane structures with diameters between 10 and 30 nm (Figure 2A). Furthermore, we identified vesicles and larger structures with internal tubular membrane structures, where the diameter of the tubules was between 15 and 25 nm (Figures S1A and 4D). No significant membrane deformation was observed with Mic10 concentrations below 200 nM, with empty vesicles, LUVs that had undergone a reconstitution protocol in the absence of protein, or LUVs with incorporated Tim23 (Figure 2A). To confirm that Mic10 induced changes in membrane morphology in bulk, we used dynamic light scattering (DLS) to measure the vesicle size distribution in response to different treatments. Only LUVs with incorporated Mic10 showed large-scale shifts in the vesicle size distribution (Figure 2B). In addition, flotated Mic10-containing liposomes from bottom layers showed more pronounced size distribution shifts than those from upper layers (Figure S1B). Similar changes could be observed with vesicles incubated with endophilin BAR domain (Figure S1C). To analyze if changes in membrane morphology can be directly correlated with membrane-integrated Mic10, we investigated the protein's effect on giant unilamellar vesicles (GUVs). Fluorescently labeled Mic10 was incorporated into LUVs, and GUVs were formed from these proteoliposomes using an electro-swelling protocol (Aimon et al., 2011; Girard et al., 2004). Incorporation of Mic10 into GUVs led to a massive accumulation of internal vesicular and tubular membrane structures. These structures were decorated evenly with Mic10 (Figures 2C and 2D), which was also observed with immuno-gold-labeled, Mic10-induced membrane tubes using electron microscopy (Figure S1F). In contrast, Tim23 was evenly distributed across GUV surfaces and did not cause membrane morphology changes (Figures 2C and 2D). These experiments show that Mic10 is able to induce high degrees of membrane curvature in model membranes with rather different physical properties.

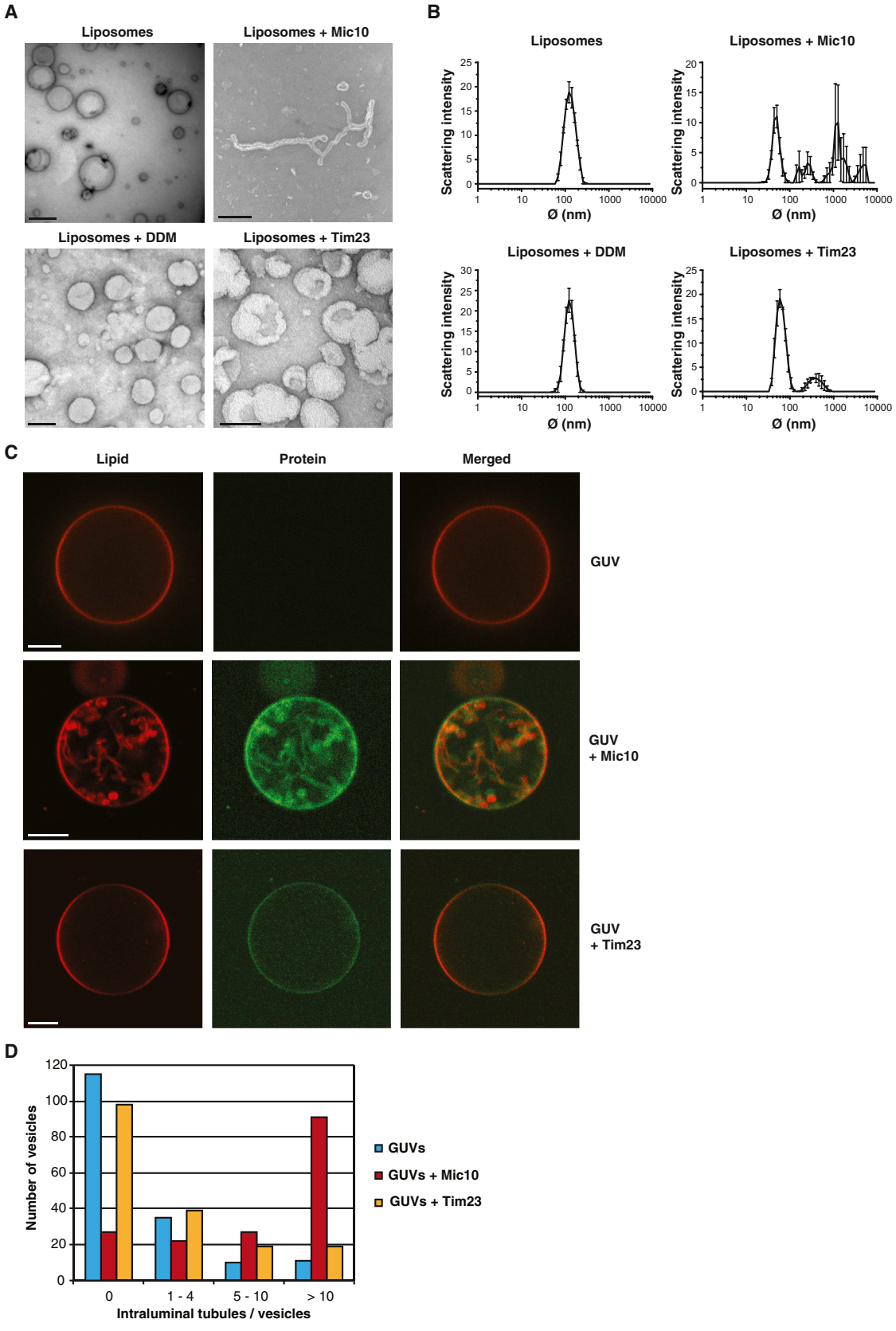

(legend on next page)

Mic10 Spans the IM in a Hairpin Topology and Forms Homo-oligomers

To unravel the molecular mechanism by which Mic10 induces membrane curvature, we first set out to determine its membrane topology. The C terminus of Mic10 has been shown before to be located to the IMS, but different views exist on the number of transmembrane segments within Mic10 (Alkhaja et al., 2012; Harner et al., 2011; von der Malsburg et al., 2011). To experimentally map the topology, we used site-directed labeling of cysteine mutants with subsequent weight shift analysis (Voeltz et al., 2006). We designed cysteine mutants that would allow us to distinguish between the two possible topologies upon labeling (Figure S2A). These constructs were expressed in yeast cells, mitoplasts were generated from purified mitochondria, and the membrane-impermeable reagent maleimide PEG (2 kDa) was added. Mitoplast integrity was tested by proteinase K digestion of several marker proteins (Figure S2B). As confirmed by weight shifts in SDS gels, cysteines at the N terminus (Figure 3A lane 9) and at the C terminus (Figure 3A lane 12) were efficiently labeled, whereas a cysteine at position 62 was not (Figure 3A lane 6). Controls showed that the outer membrane, but not the IM, was partially permeable for maleimide PEG (Figure S2C lanes 2, 4, 6, 8) and that all constructs could be labeled after mitoplasts were opened with SDS (Figure 3A lanes 5, 8, 11). We conclude that Mic10 contains two transmembrane domains and spans the IM with a hairpin topology (Figure 3B).

Membrane curvature induction often depends on clustering or oligomerization of proteins. While Mic10 is part of a large hetero-oligomeric complex, it has been proposed that the protein itself might form homo-oligomers in the IM (Harner et al., 2011). Mic10 has two highly conserved elongated GxxxG motifs in its two transmembrane domains (Figure 3C) (Alkhaja et al., 2012). Such glycine-rich motifs are known to be crucial for helix-helix packing and transmembrane domain oligomerization in lipid bilayers (Russ and Engelman, 2000). Mic10 oligomers could be detected on denaturing gels after solubilization of the protein in DDM (Figure 3D lane 2) and were obvious after western blot analysis of these samples (Figure 3D lane 3). Mic10 solubilized in mild detergents also clearly showed a range of oligomers after blue native (BN) electrophoresis (Figure 3E). Subsequently, we performed FRET (Förster resonance energy transfer) experiments of Mic10 reconstituted into liposomes (Figure 3F). We could detect efficient FRET signals when two different fractions of fluorescently labeled protein (Mic10-Alexa-488 [donor] and Mic10-Alexa-568 [acceptor]) were incorporated, confirming that Mic10 molecules are in close proximity in biological membranes.

Oligomerization of Mic10 Is a Prerequisite for Membrane Sculpting In Vitro

We next asked whether protein oligomerization could be directly linked to the induction of membrane curvature. To this end, we produced a variety of mutations within the GxxxG motifs and analyzed their oligomeric behavior using the electrophoretic assay described above (Figures 4A and 4B). Strikingly, we found that the double mutant Mic10$^{G50/52A}$ was unable to oligomerize as judged by SDS (Figure 4A lane 10) or by BN gels (Figure 4B). Moreover, almost no FRET signal of membrane-reconstituted Mic10$^{G50/52A}$ could be detected (Figure 4C), demonstrating that Mic10$^{G50/52A}$ does not form oligomers in a membrane environment.

After confirming the oligomerization deficiency of Mic10$^{G50/52A}$, we proceeded to analyze the ability of the mutant to sculpt membranes. Liposomes containing Mic10$^{G50/52A}$ displayed flotation patterns similar to empty vesicles and Tim23-containing LUVs (Figures S3A and S3B). When integrated into LUVs, the mutant failed to induce membrane curvature as assessed by electron microscopy (Figure 4D). Moreover, such proteoliposomes did not show broad changes in their vesicle size distribution as measured by DLS (Figure 4E). This clearly shows that Mic10's membrane bending activity crucially depends on its ability to oligomerize.

Mic10 Oligomerization Is a Prerequisite for Normal CJ Formation In Vivo

Together with previous localization studies showing that Mic10 resides at CJs (Harner et al., 2011; Jans et al., 2013), our observations implicate Mic10 in shaping the IM at CJs. Since oligomerization is a prerequisite for inducing curvature in model membranes, we asked whether expression of the oligomerization mutant leads to abnormal mitochondrial IM structures. We found that *mic10*Δ cells expressing Mic10$^{G50/52A}$ displayed phenotypes similar to *mic10*Δ cells with highly decreased number of CJs and about 50% altered cristae morphology (60% for mitochondria from *mic10*Δ cells) (Figures 4F–4H). Mitochondria from *mic10*Δ cells expressing wild-type Mic10 showed a mild phenotype, with 70%–80% of the mitochondria displaying wild-type cristae morphology (Figure 4H), and virtually no changes in the numbers of CJs (Figure 4G). To demonstrate that altered IM architecture is not due to a mislocalization of Mic10$^{G50/52A}$, we show that the protein was normally integrated into the MICOS complex. All MICOS subunits could be efficiently co-purified as in the case of Mic10^{WT} (Figure S3E lanes 3 and 4). When analyzing growth of the different yeast strains, we found that *mic10*Δ cells expressing wild-type Mic10 showed normal growth on non-fermentable medium, whereas *mic10*Δ cells showed strongly decreased growth phenotypes (Figure S3D) as seen before (Alkhaja et al., 2012; Harner et al., 2011; Hoppins et al., 2011; von der Malsburg et al., 2011). *mic10*Δ cells expressing Mic10$^{G50/52A}$ (Figure S3C) displayed mildly reduced growth (Figure S3D). This is probably explained by the fact that, unlike in *mic10*Δ cells, where the MICOS complex is dissociated (von der Malsburg et al., 2011), Mic10$^{G50/52A}$ is normally integrated into the complex. Collectively, these results confirm that the membrane curvature-inducing activity of Mic10, which

Figure 2. Mic10 Induces Changes of Membrane Morphology

(A) Electron micrographs of negatively stained LUVs with indicated additives (scale bars, 100 nm).

(B) Size distribution of LUVs with indicated additives analyzed by dynamic light scattering. Error bars represent SEM.

(C) GUVs (labeled with rhodamine-PE) in the absence of protein (top panel) or in the presence of Mic10 (labeled with Alexa-488) or Tim23 (labeled with Alexa-488) (scale bars, 10 μm).

(D) Histogram of the Mic10 dependence of intraluminal membrane structures of GUVs from > 100 GUVs.

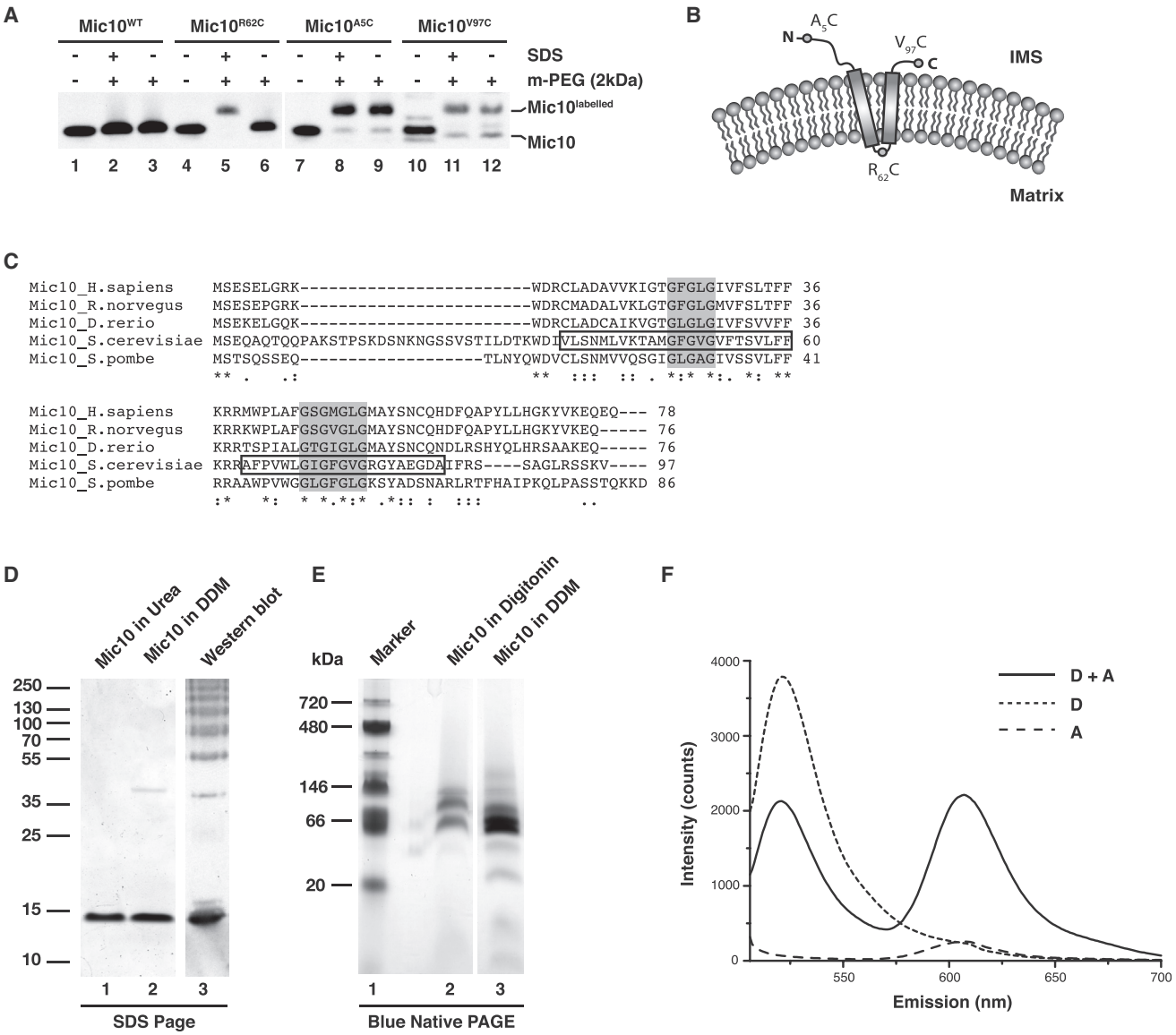

Figure 3. Topology Mapping and Oligomerization of Mic10

(A) Western blot analysis of WT and indicated cysteine mutants of Mic10 in mitoplasts in the absence and presence of SDS.

(B) Topology model of Mic10 within the IM.

(C) Sequence alignment (ClustalW) of Mic10. Black boxes mark predicted transmembrane domains. Gray boxes mark GxxxG motifs.

(D) Gel-filtrated Mic10 in urea (first lane) and in DDM (second lane and third lane) analyzed by SDS-PAGE with Coomassie brilliant blue staining (first and second lane) and western blot (third lane).

(E) Mic10 solubilized in indicated detergent and analyzed by blue native electrophoresis with Coomassie brilliant blue staining.

(F) FRET signals of Mic10 incorporated into LUVs. Mic10 acceptor labeled with Alexa-488 A and Mic10 donor labeled with Alexa-568 D.

relies on its oligomerization, is a prerequisite for normal CJ formation in mitochondria.

DISCUSSION

Mic10's hairpin topology and the ability to form homo-oligomers is reminiscent of the membrane-deforming reticulons and Yop1p/Dp1 proteins, which are crucial to generate tubular ER (Hu et al., 2008; Shibata et al., 2009; Voeltz et al., 2006). Based on these striking similarities, we hypothesize that the two transmembrane domains of Mic10 adopt an asymmetric wedge shape in the IM. This topology would allow the protein to occupy a larger surface toward the intermembrane space side of the IM and thereby generate curvature. Interestingly, with 24 amino acids, the N-terminal transmembrane domain is predicted to be unusually long. To avoid a hydrophobic mismatch, this helix might span the IM angularly and thereby account for an asymmetric wedge topology.

In addition, membrane curvature generation is often dependent on the clustering of proteins, and consistently we find that the

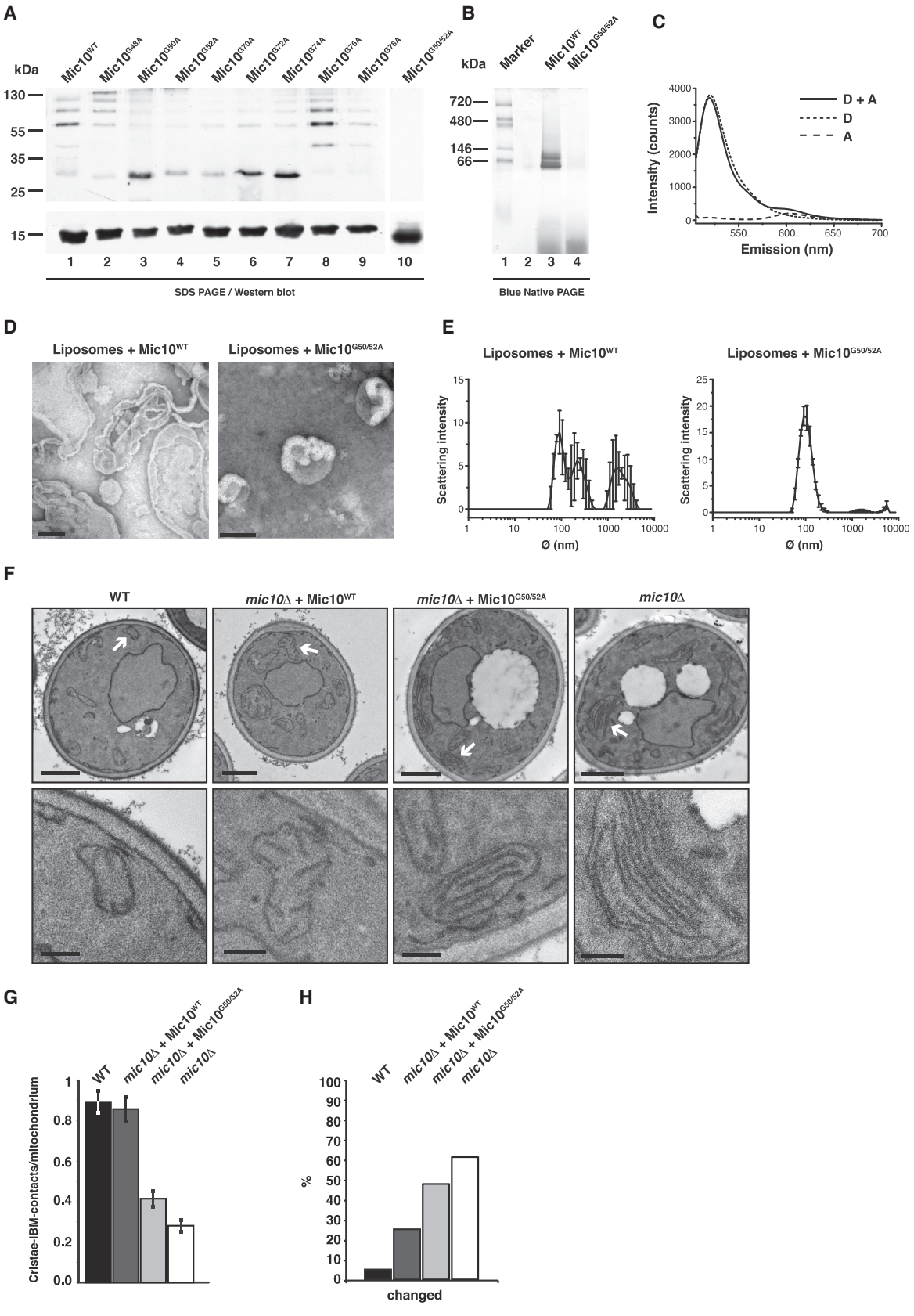

(legend on next page)

ability of Mic10 to oligomerize is a requirement for membrane sculpting in vitro and CJ formation in vivo. The fact that oligomers of Mic10 give rise to highly curved membranes is in accordance with physical considerations of membrane deformation. The energy cost per membrane area of creating a curved tubular or spherical structure can be calculated using the classical Canham, Helfrich, and Evans theory (Canham, 1970; Helfrich, 1973) by $G_{bending} = (8\pi\kappa)/(4\pi rl)$, where κ is the bending rigidity of the membrane and r and l are the tube radius and length, respectively. For soft fluid membranes, the bending rigidity was measured to be $\sim$10 k_BT (Evans and Rawicz, 1990). Although the kinetic parameters of Mic10 oligomerization are unknown, the free energy of association for other proteins with glycine-rich motifs, like glycophorin A, were measured to be $\sim$15 k_BT (Fleming et al., 1997). Assuming a comparable value for Mic10, oligomer formation could easily account for the energetic cost of membrane deformation.

In sum, our results demonstrate that Mic10 shapes the IM at CJs. Membrane structures induced by Mic10 have dimensions similar to wild-type CJs in vivo, but do not fully resemble wild-type IM architecture. This is in agreement with Mic10 being part of a multi-subunit complex and that IM morphology is not only defined by CJs but also by cristae tips, which are formed or stabilized by F_OF_1-ATPase dimers (Davies et al., 2012; Strauss et al., 2008). Possibly interplay of both MICOS and the F_OF_1-ATPase is necessary to form normal cristae morphology in vivo, with high membrane curvature regions at CJs and cristae apexes (Hoppins et al., 2011; Zick et al., 2009).

EXPERIMENTAL PROCEDURES

Liposome Preparation and Detergent-Mediated Reconstitution

The lipids L-α-phosphatidylcholine (L-α-PC), 1,2-dioleoyl-*sn*-glycero-3-phosphoethanolamine (DOPE), and cardiolipin (CL) were purchased from Avanti Polar Lipids (Alabaster). LUVs composed of L-α-PC/DOPE/cardiolipin with a molar ratio 70/15/15 were prepared by performing freeze-thaw cycles and subsequent extrusion through a 100 nm diameter polycarbonate filter (Whatman). Purified Mic10 was renatured by dialyzing against 0.05% DDM, 100 mM NaCl, 10 mM Tris (pH 8.0) (buffer R) and added to LUVs presolubilized in buffer R. Proteoliposome formation was achieved by using detergent adsorbent Bio-Beads SM-2 (Bio-Rad).

Electron Microscopy of LUVs

Proteoliposome samples were spotted on carbon-coated grids (Agar Scientific) and stained with 5% (w/v) uranyl acetate solution. Electron microscopic imaging was performed with a Jeol JEM 1011 transmission electron microscope equipped with a Gatan Orius 1000 CCD camera.

Giant Unilamellar Vesicle Preparation

GUVs were prepared as described before (Girard et al., 2004). Briefly, GUVs were generated based on the electroformation technique described by Angelova (Angelova and Dimitrov, 1986). Preformed proteoliposomes were resuspended in low-salt buffer (5 mM NaCl, 10 mM HEPES/Tris [pH 7.4]) to a final lipid concentration of 0.5 mg/ml. One-microliter droplets were deposited on indium tin oxide (ITO)-coated glass slides. The proteoliposomes were partially dehydrated for 2 hr in a desiccator under saturated vapor pressure of a saturated KCl solution. A GUV generation chamber was assembled by separating two ITO-coated slides by 600 μl of a 300 mM glucose solution and a thin rubber spacer. For electroformation, an AC electric field was generated by a pulse generator connected to the slides. The field was applied for 3 hr across the chamber and incremented continuously from 20 mV to 1.1 V at 12 Hz frequency. Finally, the AC frequency was lowered to 4 Hz at 2 V for 30 min. This leads to detachment of the vesicles from the glass slides. GUVs were carefully collected and used immediately for visualization.

FRET Assay

A5C mono-cysteine mutants of $Mic10^{WT}$ and $Mic10^{G50/52A}$ were labeled in a denatured state with Alexa-Fluor-488 (A488) and -568 (A568) maleimide fluorophores from Life Technologies as donor and acceptor pair in 25× molar excess. Unilamellar vesicles were formed as described above. Equal amounts of both fluorophore-labeled proteins were incorporated into liposomes using 0.5% DDM and Bio-Beads in 15:1 Bio-Beads:DDM ratio. For control samples with only one fluorophore, the protein concentration was adjusted by addition of the specific protein without cysteine mutation. Final liposome concentration was 1 mg/ml.

FRET measurements were carried out using a Hitachi F-7000 fluorometer. Excitation wavelength was set to 493 nm (for FRET-pair and A488-labeled Mic10 control) and 574 nm (for FRET-pair and A568-labeled Mic10 control) for emission scans. Emission was recorded between 470 nm and 700 nm at 60 nm/min.

Topology Experiments

Maleimide PEG 2 kDa (Sigma Aldrich) modification experiments were performed on isolated swollen mitochondria (mitoplasts), which were successfully obtained by washing with 20 mM Tris (pH 7.4) buffer. The samples were incubated with 5 mM maleimide PEG 2 kDa per 20 μg mitochondria either with or without 2% SDS at 25°C, 2 hr, 600 rpm. The reactions were stopped by incubating with 25 mM DTT for 30 min. The labeling success was monitored by SDS-PAGE and subsequent western blotting.

Electron Microscopy of Yeast Cells

For electron microscopy, the yeast cells were grown at 30°C in liquid SGG medium (0.5 g/l yeast extract, 6.7 g/l yeast nitrogen base, 2 g/l −HIS dropout mix (Sherman, 2002), 30 ml/l glycerol, 1 g/l glucose) and harvested in the logarithmic growth phase. The yeast cells were fixed for 20 min in 1.5% potassium permanganate as previously described (Erdmann et al., 1989) and post-stained with 1% uranyl acetate for 2 hr. After dehydration in a graded ethanol series, the cells were embedded in epoxide resin (Agar 100; Plano). Ultrathin sections were examined using a Philips CM 120 transmission electron microscope (FEI Europe).

Statistical Analysis

Error bars for DLS data and analysis of the mitochondrial IM structure represent the standard error of the mean (SEM). DLS data were obtained from at

Figure 4. Mic10 Oligomerization Occurs through Glycine-Rich Motifs and Is a Prerequisite for Membrane Curvature Induction and Normal Cristae Junction Formation

(A) Gel-filtrated Mic10 mutants (as indicated) analyzed by SDS-PAGE with western blotting.
(B) Mic10 solubilized in DDM and analyzed by blue native electrophoresis with Coomassie brilliant blue staining.
(C) FRET signals of $Mic10^{G50/52A}$ incorporated into LUVs. Mic10 acceptor labeled with Alexa-488 A and Mic10 donor labeled with Alexa-568 D.
(D) Electron micrographs of negatively stained LUVs with incorporated $Mic10^{WT}$ (left) and $Mic10^{G50/52A}$ (right) (scale bars, 100 nm).
(E) Size distribution of LUVs with incorporated $Mic10^{WT}$ (left) and $Mic10^{G50/52A}$ (right) analyzed by dynamic light scattering. Error bars represent SEM.
(F) Representative electron microscopy images of yeast cells (top panel/scale bars, 1 μm) (indicated genetic background) and mitochondrial ultra-structures (bottom panel/scale bars, 200 nm).
(G) Quantification of cristae junctions per mitochondrion as detected in cell section. Error bars represent SEM.
(H) Quantitative evaluation of the inner mitochondrial membrane ultra-structure as detected in cell sections (wild-type and changed inner membrane structure as depicted in Figure S4).

least three independent experiments. Each experiment is averaged over at least 20 repetitive measurements.

Analysis of yeast mitochondrial ultra-structure was made from the following: Mic10WT, 275 mitochondrial sections in 101 cell images; *mic10*Δ + Mic10WT, 459 mitochondrial sections in 138 cell images; *mic10*Δ + Mic10$^{G50/52A}$, 473 mitochondrial sections in 166 cell images; *mic10*Δ, 459 mitochondrial sections in 138 cell images.

SUPPLEMENTAL INFORMATION

Supplemental Information includes Supplemental Experimental Procedures, and four figures and can be found with this article online at http://dx.doi.org/10.1016/j.cmet.2015.04.006.

ACKNOWLEDGMENTS

We thank P. Rehling for continuous discussions and advice; I. Schäfer, N. McGlincy, and J. Jethwa for helpful comments on the manuscript; and N. Pfanner and P. Rehling for materials. This work was supported by the Deutsche Forschungsgemeinschaft: SFB 803 project B09 and FOR 1905 project TP1 (M.B., N.D., and M.M.) and Center for Nanoscale Microscopy and Molecular Physiology of the Brain (S.J.).

Received: December 17, 2014
Revised: March 6, 2015
Accepted: April 1, 2015
Published: May 5, 2015

REFERENCES

Aimon, S., Manzi, J., Schmidt, D., Poveda Larrosa, J.A., Bassereau, P., and Toombes, G.E. (2011). Functional reconstitution of a voltage-gated potassium channel in giant unilamellar vesicles. PLoS ONE *6*, e25529.

Alkhaja, A.K., Jans, D.C., Nikolov, M., Vukotic, M., Lytovchenko, O., Ludewig, F., Schliebs, W., Riedel, D., Urlaub, H., Jakobs, S., and Deckers, M. (2012). MINOS1 is a conserved component of mitofilin complexes and required for mitochondrial function and cristae organization. Mol. Biol. Cell *23*, 247–257.

Angelova, M.I., and Dimitrov, D.S. (1986). Liposome Electroformation. Faraday Discuss. *81*, 303–311.

Canham, P.B. (1970). The minimum energy of bending as a possible explanation of the biconcave shape of the human red blood cell. J. Theor. Biol. *26*, 61–81.

Davies, K.M., Anselmi, C., Wittig, I., Faraldo-Gómez, J.D., and Kühlbrandt, W. (2012). Structure of the yeast F1Fo-ATP synthase dimer and its role in shaping the mitochondrial cristae. Proc. Natl. Acad. Sci. USA *109*, 13602–13607.

Erdmann, R., Veenhuis, M., Mertens, D., and Kunau, W.H. (1989). Isolation of peroxisome-deficient mutants of Saccharomyces cerevisiae. Proc. Natl. Acad. Sci. USA *86*, 5419–5423.

Evans, E., and Rawicz, W. (1990). Entropy-driven tension and bending elasticity in condensed-fluid membranes. Phys. Rev. Lett. *64*, 2094–2097.

Farsad, K., Ringstad, N., Takei, K., Floyd, S.R., Rose, K., and De Camilli, P. (2001). Generation of high curvature membranes mediated by direct endophilin bilayer interactions. J. Cell Biol. *155*, 193–200.

Fleming, K.G., Ackerman, A.L., and Engelman, D.M. (1997). The effect of point mutations on the free energy of transmembrane alpha-helix dimerization. J. Mol. Biol. *272*, 266–275.

Gallop, J.L., Jao, C.C., Kent, H.M., Butler, P.J., Evans, P.R., Langen, R., and McMahon, H.T. (2006). Mechanism of endophilin N-BAR domain-mediated membrane curvature. EMBO J. *25*, 2898–2910.

Girard, P., Pécréaux, J., Lenoir, G., Falson, P., Rigaud, J.L., and Bassereau, P. (2004). A new method for the reconstitution of membrane proteins into giant unilamellar vesicles. Biophys. J. *87*, 419–429.

Harner, M., Körner, C., Walther, D., Mokranjac, D., Kaesmacher, J., Welsch, U., Griffith, J., Mann, M., Reggiori, F., and Neupert, W. (2011). The mitochondrial contact site complex, a determinant of mitochondrial architecture. EMBO J. *30*, 4356–4370.

Helfrich, W. (1973). Elastic properties of lipid bilayers: theory and possible experiments. Z. Naturforsch. C *28*, 693–703.

Hoppins, S., Collins, S.R., Cassidy-Stone, A., Hummel, E., Devay, R.M., Lackner, L.L., Westermann, B., Schuldiner, M., Weissman, J.S., and Nunnari, J. (2011). A mitochondrial-focused genetic interaction map reveals a scaffold-like complex required for inner membrane organization in mitochondria. J. Cell Biol. *195*, 323–340.

Hu, J., Shibata, Y., Voss, C., Shemesh, T., Li, Z., Coughlin, M., Kozlov, M.M., Rapoport, T.A., and Prinz, W.A. (2008). Membrane proteins of the endoplasmic reticulum induce high-curvature tubules. Science *319*, 1247–1250.

Jans, D.C., Wurm, C.A., Riedel, D., Wenzel, D., Stagge, F., Deckers, M., Rehling, P., and Jakobs, S. (2013). STED super-resolution microscopy reveals an array of MINOS clusters along human mitochondria. Proc. Natl. Acad. Sci. USA *110*, 8936–8941.

John, G.B., Shang, Y., Li, L., Renken, C., Mannella, C.A., Selker, J.M., Rangell, L., Bennett, M.J., and Zha, J. (2005). The mitochondrial inner membrane protein mitofilin controls cristae morphology. Mol. Biol. Cell *16*, 1543–1554.

Mannella, C.A. (2006). Structure and dynamics of the mitochondrial inner membrane cristae. Biochim. Biophys. Acta *1763*, 542–548.

Meinecke, M., Wagner, R., Kovermann, P., Guiard, B., Mick, D.U., Hutu, D.P., Voos, W., Truscott, K.N., Chacinska, A., Pfanner, N., and Rehling, P. (2006). Tim50 maintains the permeability barrier of the mitochondrial inner membrane. Science *312*, 1523–1526.

Meinecke, M., Boucrot, E., Camdere, G., Hon, W.C., Mittal, R., and McMahon, H.T. (2013). Cooperative recruitment of dynamin and BIN/amphiphysin/Rvs (BAR) domain-containing proteins leads to GTP-dependent membrane scission. J. Biol. Chem. *288*, 6651–6661.

Pellegrini, L., and Scorrano, L. (2007). A cut short to death: Parl and Opa1 in the regulation of mitochondrial morphology and apoptosis. Cell Death Differ. *14*, 1275–1284.

Pfanner, N., van der Laan, M., Amati, P., Capaldi, R.A., Caudy, A.A., Chacinska, A., Darshi, M., Deckers, M., Hoppins, S., Icho, T., et al. (2014). Uniform nomenclature for the mitochondrial contact site and cristae organizing system. J. Cell Biol. *204*, 1083–1086.

Rabl, R., Soubannier, V., Scholz, R., Vogel, F., Mendl, N., Vasiljev-Neumeyer, A., Körner, C., Jagasia, R., Keil, T., Baumeister, W., et al. (2009). Formation of cristae and crista junctions in mitochondria depends on antagonism between Fcj1 and Su e/g. J. Cell Biol. *185*, 1047–1063.

Russ, W.P., and Engelman, D.M. (2000). The GxxxG motif: a framework for transmembrane helix-helix association. J. Mol. Biol. *296*, 911–919.

Scheffler, I.E. (2007). Mitochondria (Hoboken, NJ: Wiley).

Scorrano, L., Ashiya, M., Buttle, K., Weiler, S., Oakes, S.A., Mannella, C.A., and Korsmeyer, S.J. (2002). A distinct pathway remodels mitochondrial cristae and mobilizes cytochrome c during apoptosis. Dev. Cell *2*, 55–67.

Sherman, F. (2002). Getting started with yeast. Methods Enzymol. *350*, 3–41.

Shibata, Y., Hu, J., Kozlov, M.M., and Rapoport, T.A. (2009). Mechanisms shaping the membranes of cellular organelles. Annu. Rev. Cell Dev. Biol. *25*, 329–354.

Strauss, M., Hofhaus, G., Schröder, R.R., and Kühlbrandt, W. (2008). Dimer ribbons of ATP synthase shape the inner mitochondrial membrane. EMBO J. *27*, 1154–1160.

Voeltz, G.K., Prinz, W.A., Shibata, Y., Rist, J.M., and Rapoport, T.A. (2006). A class of membrane proteins shaping the tubular endoplasmic reticulum. Cell *124*, 573–586.

Vogel, F., Bornhövd, C., Neupert, W., and Reichert, A.S. (2006). Dynamic subcompartmentalization of the mitochondrial inner membrane. J. Cell Biol. *175*, 237–247.

von der Malsburg, K., Müller, J.M., Bohnert, M., Oeljeklaus, S., Kwiatkowska, P., Becker, T., Loniewska-Lwowska, A., Wiese, S., Rao, S., Milenkovic, D., et al. (2011). Dual role of mitofilin in mitochondrial membrane organization and protein biogenesis. Dev. Cell *21*, 694–707.

Zick, M., Rabl, R., and Reichert, A.S. (2009). Cristae formation-linking ultrastructure and function of mitochondria. Biochim. Biophys. Acta *1793*, 5–19.

Cell Metabolism

Supplemental Information

Mic10 Oligomerizes to Bend Mitochondrial Inner Membranes at Cristae Junctions

Mariam Barbot, Daniel C. Jans, Christian Schulz, Niels Denkert, Benjamin Kroppen, Michael Hoppert, Stefan Jakobs, and Michael Meinecke

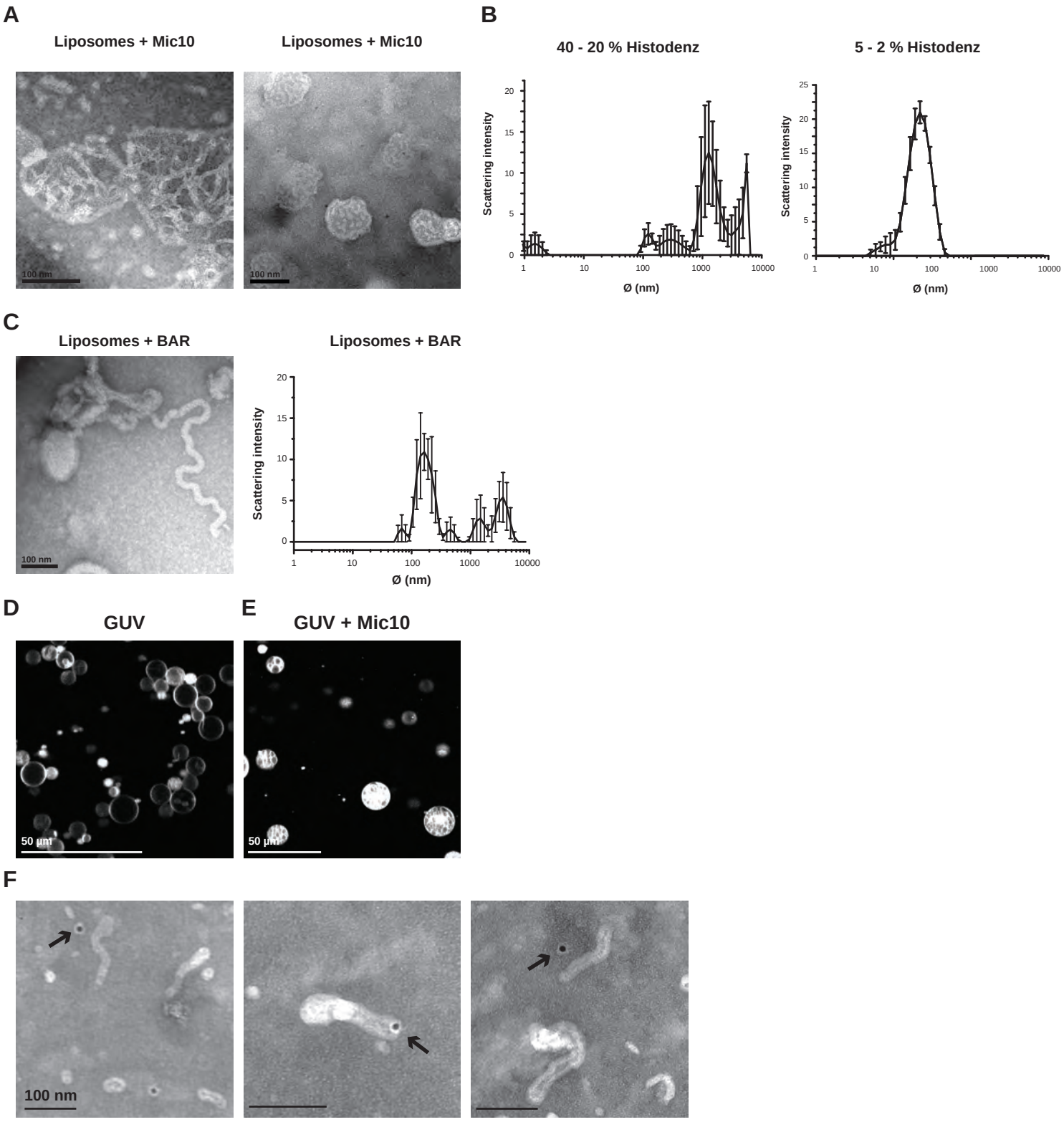

Figure S1. Vesicle deformation.
(A) Tubular membrane structures as observed after reconstitution of Mic10 into LUVs (scale bar 100 nm).
(B) Size distribution of Mic10 containing LUVs after flotation assay. Indicated layers were analyzed by dynamic light scattering. Error bars represent SEM.
(C) Membrane deformation of LUVs by endophilin BAR domain (scale bar 100 nm)(left). Size distribution of LUVs after incubation with endophilin BAR domain analyzed by dynamic light scattering (right). Error bars represent SEM.
(D) GUVs generated from LUVs by electroswelling (scale bar 50 µm).
(E) GUVs generated from Mic10 containing LUVs by electroswelling (scale bar 50 µm).
(F) Mic10 induced membrane tubules after immuno-gold labeling of Mic10 (arrows indicate gold particles which can be up to ~20 nm away from the epitope due to the size of the linking antibodies.)

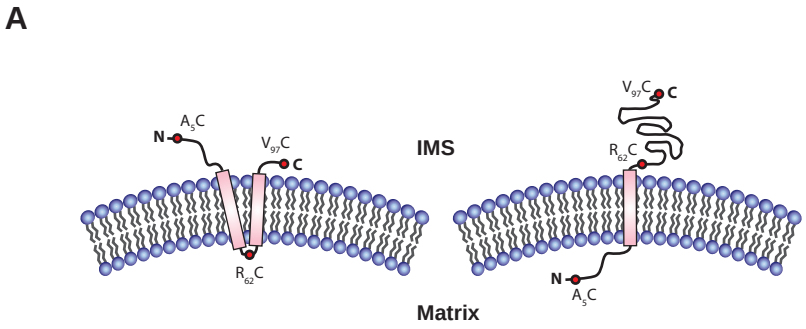

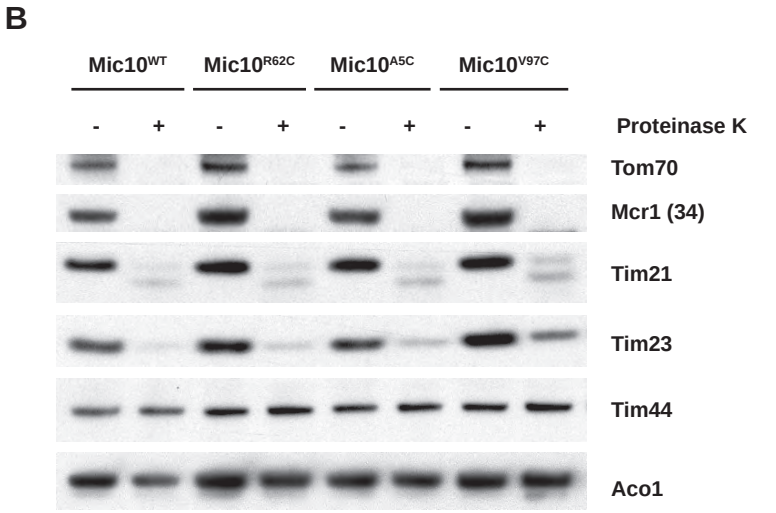

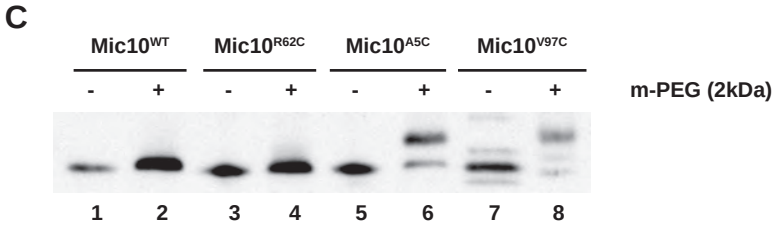

Figure S2. Topology of Mic10 in the mitochondrial inner membrane.

(A) Cartoon of the different possibilities how Mic10 spans the inner membrane with either one or two transmembrane helices under the assumption that the C-terminus is located within the intermembrane space.

(B) Mitochondria isolated from mic10Δ + Mic10WT, mic10Δ + Mic10^{R62C}, mic10Δ + Mic10^{A5C} and mic10Δ + Mic10^{V97C} cells were subjected to hypoosmotic treatment (swelling) and Proteinase K (Prot. K) digestion where indicated. Samples were analysed by SDS-PAGE and immunodecoration. Tom70 and Mcr1 are outer membrane proteins whereas Tim44 and Aco1 are located in the mitochondrial matrix. Tim23 and Tim21 are both integral inner membrane proteins but antibodies are directed against their IMS part.

(C) Western blot analysis of WT and indicated cysteine mutants of Mic10 in un-swollen mitochondria. Lanes 6 and 8 indicate that the OM is partially permeable for m-PEG. Lane 4 shows that the IM is not permeable for m-PEG.

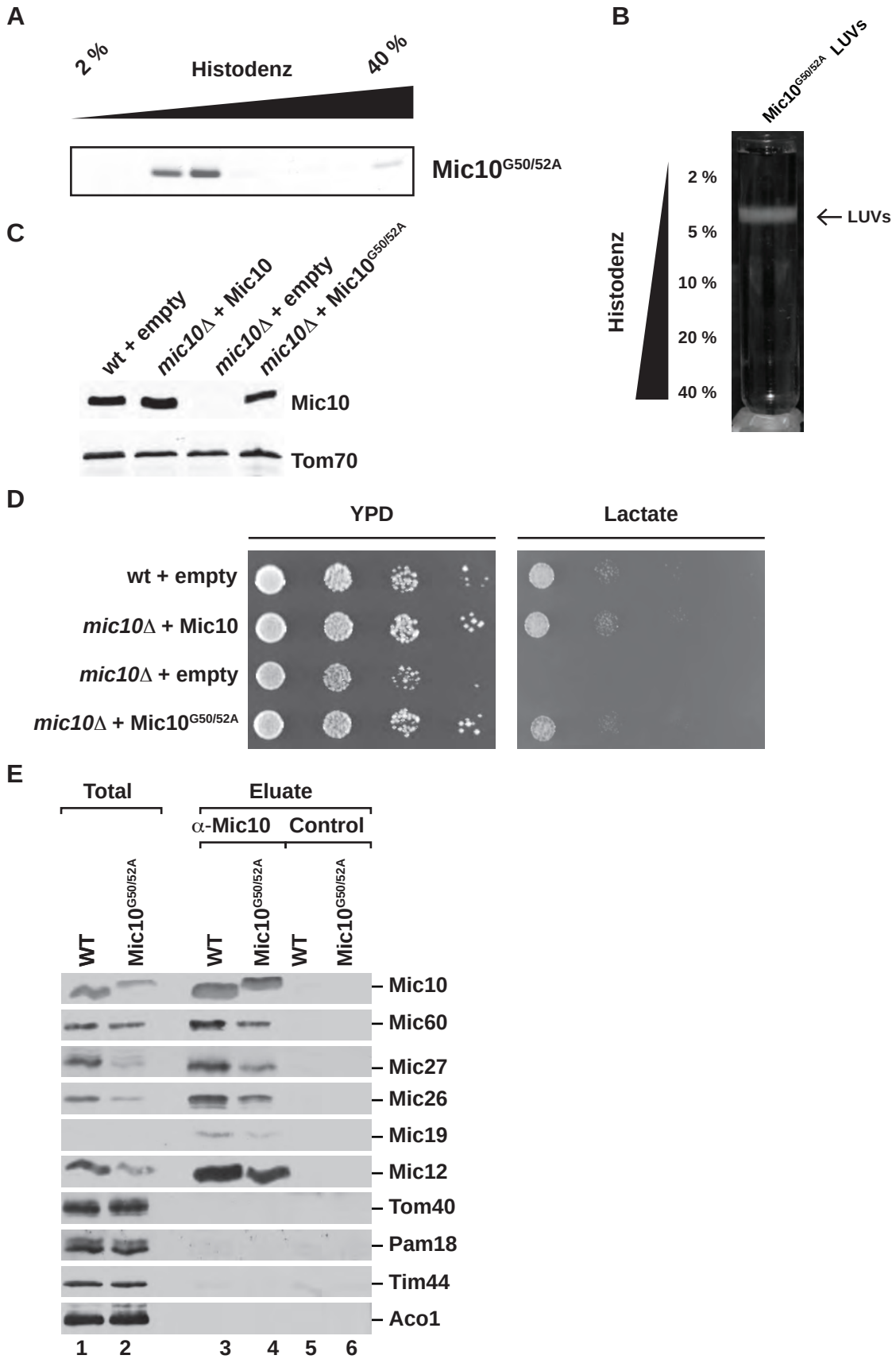

Figure S3. Mic10G50/52A can be reconstituted into model membranes and is normally inserted into the MICOS complex.

(A) Coomassie stained SDS gel of the fractionated density gradient flotation shown in (B).

(B) Flotation assay of Mic10G50/52A containing LUVs.

(C) Steady state levels of different Mic10 variants expressed in yeast cells analyzed by Western blot (upper panel). The outer mitochondrial protein Tom70 was used as a loading control (bottom panel).

(D) Growth test of indicated Mic10 strains on glucose (left) and lactate (right).

(E) Co-purification of MICOS subunits with Mic10WT (lane 3) and Mic10G50/52A (lane 4). All MICOS subunits are co-purified by both Mic10 variants whereas no control proteins are detectable after co-immunoprecipitation.

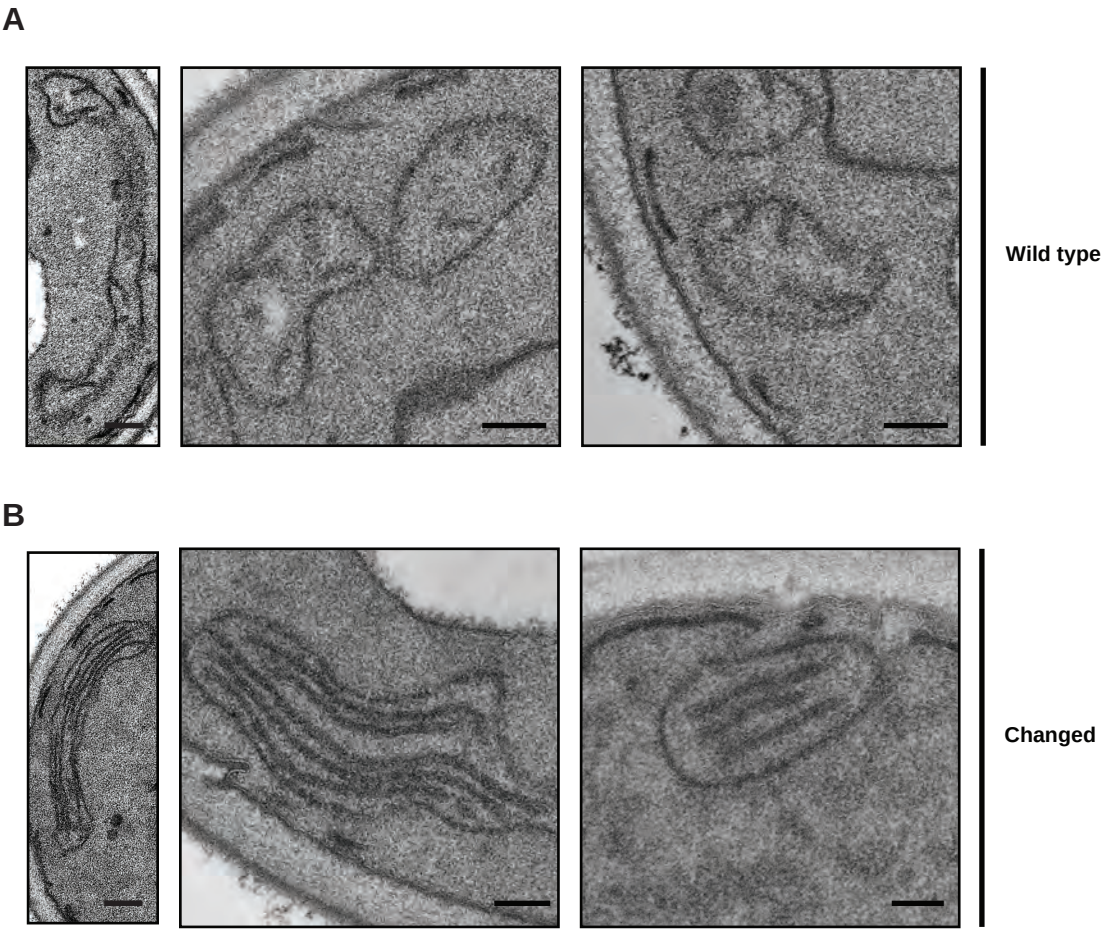

Figure S4. Mitochondrial morphology.
Representative images of mitochondria that serve as a baseline to distinguish between wild type (A) and changed (B) inner membrane morphology.

Supplemental Information

Supplemental Experimental Procedures

Cloning and expression of Mic10. Primers containing relevant restriction enzyme sites were used for polymerase chain reaction (PCR) to generate yeast Mic10. The PCR product was successfully cloned into pPROEX HTC vector containing N-terminal His_6-tag. After expression of Mic10 in *E. coli* strain BL21(DE3) (1 mM isopropyl-β-D-thiogalactopyranoside (IPTG), 3h, 37°C) cells were lysed, inclusion bodies were isolated (Meinecke et al., 2006) and subsequently dissolved in resuspension buffer containing 8 M urea, 100 mM NaCl, 10 mM Tris-HCl, 2 mM DTT, pH 8.0. The mixture was applied to the NiNTA-agarose column and eluted with resuspension buffer supplemented with 500 mM imidazole. Isolated Mic10 was further subjected on HiLoad 16/600 Superdex 200 size exclusion column (GE Healthcare, Piscataway, NJ, USA). Separated fractions were analyzed by SDS-PAGE and immunoblotting.
All single mutants G48A, G50A, G52A, G70A, G72A, G74A, G76A, G78A and a double mutant G50A/G52A were obtained by site-directed mutagenesis. The overexpressed mutant proteins were subjected to the same purification steps as the wild type protein.

Liposome flotation assay and carbonate extraction. For density flotation assays, nonionic Histodenz (SIGMA-ALDRICH) 40/20/10/5/2 percent gradients were prepared in 100 mM NaCl, 10 mM Tris, pH 8.0 buffer. Proteoliposomes were loaded below the 40 % layer, centrifuged at 150,000 x g for 45 min and ultimately collected at the interfaces of the layers. It should be noted that 45 min is not enough to reach equilibrium of flotated samples. Therefore, the different layers likely correspond to different shapes (different surface to volume ratios) of the deformed vesicles. After precipitation with 10 % trichloroacetic acid (TCA) the samples were resuspended in SDS sample buffer and subjected for SDS-PAGE analysis.
For sodium carbonate extraction assay proteoliposomes collected from the interfaces were treated by 20 mM Na_2CO_3 and incubated for 30 min on ice. Samples were centrifuged at 150,000 x g for 45 min and the supernatants were TCA precipitated. Ultimately, membrane and TCA pellets were resuspended in SDS sample buffer and analyzed by SDS-PAGE.

Dynamic light scattering. Samples were measured using a Zetasizer Nano S (Malvern Instruments). Data were obtained from at least three independent measurements. Each measurement consists of 20 repetitions over 10 minutes. Errors were calculated as the standard deviation from the averaged values.

Blue native electrophoresis. Approximately 2.5 µg of $Mic10^{WT}$ and $Mic10^{G50/52A}$ in buffer R were mixed with 20:1 v/v 5 % Coomassie G-250 and NativePAGE 4x sample buffer (Invitrogen) and separated on a NativePAGE 3-12 % Bis-Tris gel (Invitrogen) at a constant 150 V. One third of the electrophoresis was performed with pre-chilled dark blue cathode buffer and the rest with light blue cathode buffer. The bands were visualized by Coomassie G-250 staining.

Yeast strains and growth. The *mic10* open reading frame was cloned into pRS413 under the control of its native promoter and terminator. Mutants were generated by site-directed mutagenesis. *mic10*Δ (Mat a, his3-Δ1 leu2Δ0 met15Δ0 ura3Δ0; mio10::kanMX4) (Open Biosystems, Thermo Biosystems, Huntsville, AL) cells were either transformed with the empty plasmid or plasmids containing wild type or respective mutant alleles of *mic10*. The expression was verified by whole cell extracts, SDS-PAGE and Western blotting. Cell growth

was assessed by spotting serial dilutions on selective glucose or Lactate plates (0.67 % yeast nitrogen base without amino acids, 0.07 % complete supplement mixture lacking Histidine (MP Biomedicals), 25 g/l agar and 2% glucose or 3 % Lactate, pH 5.0) and incubation at 30°C or 18°C, respectively.

Immunogold staining of Mic10 proteoliposomes. Mic10 containing liposomes were shortly spotted on carbon-coated grids (Agar scientific, Essex) and transferred to drops of Tris-Buffered Saline (TBS) washing solution. Afterwards, the grids were incubated with the primary anti-His antibody (Sigma-Aldrich) 1:6000 dilution for 1hour at 25°C followed by washing and subsequent incubation with the secondary Anti-Mouse IgG- Gold (colloidal gold 10 nm) antibody (Sigma-Aldrich) 1:100 dilution for 45 min at 25°C as recommended by manufacturers. Subsequently, the grids were washed with TBS and eventually stained with 5 % (w/v) uranyl acetate solution. Electron microscopic imaging was performed as described above.

Construction of cysteine mutants and preparation of mitochondria. All Mic10 cysteine mutants R62C, A5C and V97C were obtained by site-directed mutagenesis from the plasmid containing wild type alleles of *MIC10*. The resulting plasmids and plasmid containing wild type Mic10 were transformed into a *mic10*Δ strain (Mat a, his3-Δ1 leu2Δ0 met15Δ0 ura3Δ0; mio10::kanMX4) (Open Biosystems, Thermo Biosystems, Huntsville, AL, USA) using the lithium acetate method.
Mitochondria were isolated by using Zymolyase treatment, Dounce homogenization, and subsequent differential centrifugation according to Meisinger et al. (2006) (Meisinger et al., 2006) from cells grown on selective 3% glycerol media (0.67 % yeast nitrogen base without amino acids, 0.07 % complete supplement mixture lacking Histidine (MP Biomedicals).

Mic10 co-immunoprecipitation. Mitochondria were solubilised in 20 mM Tris-HCl pH 7.4, 100 mM NaCl, 10% glycerol, 0.5 mM EDTA and 1 % digitonin. The supernatant obtained after centrifugation was loaded on ProteinA sepharose coupled with a-Mic10 serum. After binding the beads were washed with solubilization buffer containing 0.3 % digitonin and bound proteins were eluted with 100 mM glycine pH 2.8. Samples were analyzed by SDS-PAGE and Western blotting.

References

Meisinger, C., Pfanner, N., and Truscott, K.N. (2006). Isolation of yeast mitochondria. Methods Mol. Biol. *313*, 33–39.